Bull. Mater. Sci., Vol. 33, No. 4, August 2010, pp. 501–508. © Indian Academy of Sciences.

Effect of carbon on corrosion resistance of powder-processed Fe–0·35%P alloys

YASHWANT MEHTA*, SHEFALI TRIVEDI[‡], K CHANDRA[†] and P S MISHRA[†]

Metallurgical and Materials Engineering Department, National Institute of Technology Srinagar, Srinagar 190 006, India
[†]Metallurgical and Materials Engineering Department, Indian Institute of Technology, Roorkee 247 667, India
[‡]Department of Mechanical Engineering, Indian Institute of Technology, New Delhi 110 016, India

MS received 17 March 2009; revised 28 April 2009

Abstract. **The corrosion behaviour of phosphoric irons containing 0·35 wt % P, 2% copper, 2% nickel, 1% silicon, 0·5% molybdenum, with/without 0·15% carbon prepared by powder forging route were studied in different environments. The various environments chosen were acidic (0·25 M H_2SO_4 solution of pH 0·6), neutral/marine (3·5% NaCl solution of pH 6·8) and alkaline (0·5 M Na_2CO_3 + 1·0 M $NaHCO_3$ solution of pH 9·4). The corrosion studies were conducted using Tafel extrapolation and linear polarization methods. The studies also compare Armco iron with phosphoric irons. It was observed that the addition of carbon improved the corrosion resistance of a Fe–0·35%P–2%Ni–2%Cu–1%Si–0·5%Mo alloy in all the environments. Corrosion rates were highest in acid medium, minimal in alkaline medium and low in neutral solution. SEM/EDAX was used to characterize the compositions.**

Keywords. **Phosphoric iron; corrosion; powder metallurgy; forged; ancient iron.**

1. Introduction

In contrast to carbon steel, ancient phosphoric irons that were used for constructing large beams and located at Konark and Puri in India, have revealed excellent atmospheric corrosion resistance in saline seashore environments for several hundred years (Balasubramaniam 2002). The 1600-year-old Delhi iron pillar is a living testimony to the remarkable corrosion resistance of phosphoric irons. The presence of relatively high phosphorus, 0·25 wt %, in the Pillar plays a major role in its excellent corrosion resistance by facilitating the formation of a protective passive film on the surface (Balasubramaniam 2000; Balasubramaniam and Ramesh Kumar 2000).

Corrosion of iron or steel is affected by exposed environment (Fontana 2006). Corrosion depends on both, the composition of the metal/alloy and the environmental conditions. One of the important electrolyte variables affecting corrosion of iron is pH, while other variables are concentration, fluid flow, temperature and oxidizing power of the solution (Lorbeer and Lorenz 1980).

The diffusion controlled oxygen reduction predominates in weak acid and neutral solutions. The corrosion rate is dependent on hydrogen ion concentration in case of acidic solutions (Lorbeer and Lorenz 1980).

The steel (2·0 wt. % Si) showed high corrosion resistance compared to carbon steel (Si–Mn) in the wet/dry cyclic corrosion test with chloride ions (Nishimura 2008). Addition of 3·75% nickel or 0·675% copper is beneficial in wet/dry or continuously wet marine conditions (Oakwood 1987).

An attempt, therefore, needs to be made to understand the role of carbon in phosphoric irons especially when other alloying elements are present. In this paper, the corrosion behaviour of two phosphoric irons with/without 0·15 wt% C processed by powder metallurgy has been investigated in three different solutions.

2. Experimental

For making Fe–P–Cu–Mo–Ni–Si (with or without carbon) alloys by powder metallurgical technique, ferro-phosphorus, ferro-silicon and ferro-molybdenum powders were prepared separately by grinding lumps of ferro-phosphorus, ferro-silicon, ferro-molybdenum (containing 22% P, 70% Si, 60% Mo, respectively) with the help of mortar and pestle (iron) or filing. Powders with –200 mesh size were employed for the preparation of alloys. Pure copper and nickel powders having –200 mesh sizes were taken for preparation of these alloys. We have used natural crystalline graphite (containing about 80% C) which is considered to be the most suitable for the purpose of alloying with iron. Further, in powder metallurgy about 60% of this C was utilized for the purpose of alloying. Rest of the iron converts itself into reducing gases which clean the surfaces of iron powder particles (Sands

*Author for correspondence (yashwant.mehta@gmail.com)

Table 1. Composition of phosphoric irons developed in the study and Armco iron.

Sample	P (wt %)	Ni (wt %)	Cu (wt %)	Si (wt %)	Mo (wt %)	C (wt %)	Fe
1 (Armco)	–	–	–	–	–	–	>99%
2	0·35	2·0	2·0	1·0	0·5	–	Balance
3	0·35	2·0	2·0	1·0	0·5	0·15	Balance

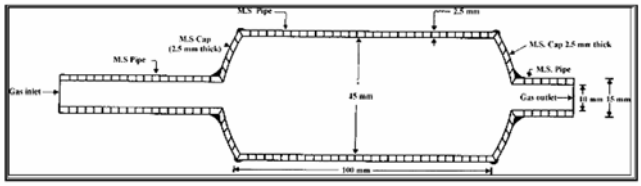

Figure 1. Cross-section of mild steel capsule used in the present investigation.

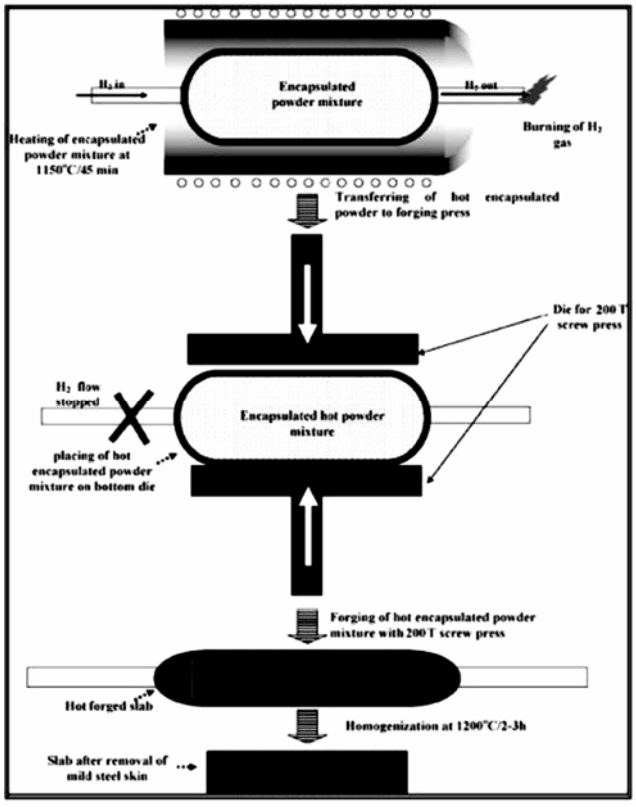

Figure 2. Schematic diagram illustrating the production of slab by hot forging of encapsulated powder mixture.

and Shakespeare 1966). Accordingly, the dissolved C content in our alloy system was expected to be about 0·072 wt %.

The powder blends were manually mixed to make desired alloy chemistry. About 500 g of each blended mixture was then poured into a mild steel capsule (as shown in figure 1). The encapsulated powders were heated in a tubular furnace at 1150°C for 45 min in dry

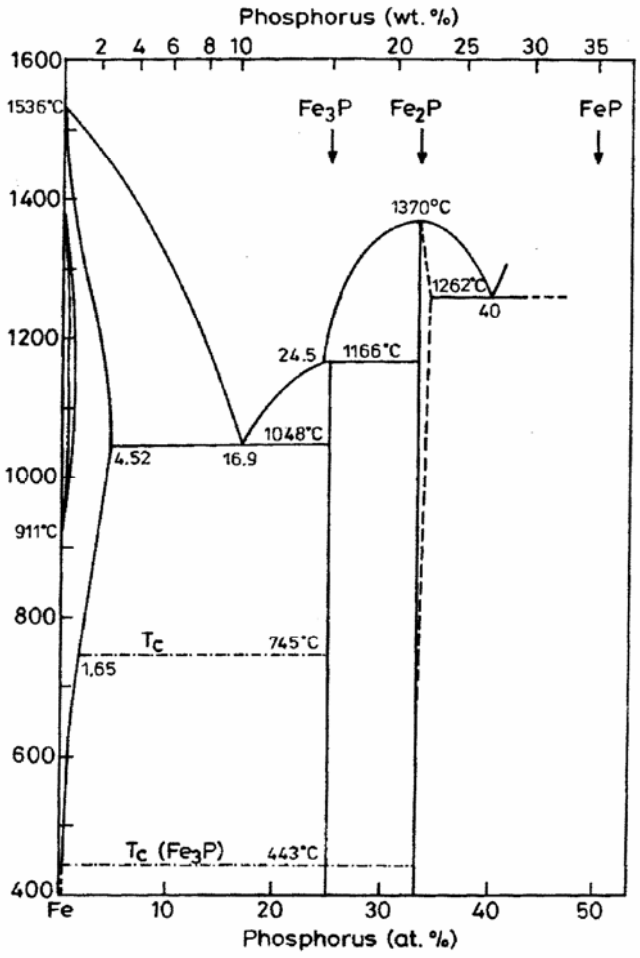

Figure 3. Fe–P binary phase diagram (Kubaschewski 1982).

hydrogen atmosphere in order to remove the oxide layer from the surfaces of the powder particles. Heated capsules were then forged with a 200T capacity friction screw press to make slabs using a channel die. Two alloys processed by powder metallurgy were made in the present investigation. These are given in table 1.

The compositions of these alloys are based on the powder mixture. Figure 2 schematically illustrates the process of making slabs through hot powder forging technique. The slabs were then homogenized at 1200°C for 3 h to eliminate compositional inhomogeneity. Alloys were heated for 3 h because diffusion of silicon in iron is much slower than the other alloying elements.

All the alloying elements are present in the form of fine particles around pure iron particles. This pure iron

particle is 100% gamma-phase at the homogenizing temperature of 1200°C as per the Fe–P phase diagram proposed by Kubaschewski (1982) (figures 3 and 4). Phosphorous (in the form of ferro-phosphorous) combines with this gamma iron powder particle and dissolves in it. As it dissolves, it gets converted into ferrite (figures 3 and 4) and as ferrite phase grows out of gamma phase, more and more phosphorous penetrates into it. This helps carry all the other alloying elements in ferrite phase with the exception of carbon. This is because carbon has very low solubility in ferrite. Consequently carbon is pushed towards gamma rich region (Erhart and Grabke 1981). As the homogenization proceeds, clear partitioning of alloying elements between ferrite and gamma iron takes place. At the end of homogenization, a major portion of carbon segregates in gamma iron region whereas the other alloying elements are concentrated in the ferrite region. After completion of homogenization and lowering of temperatures during furnace cooling there is no gamma phase left as per the equilibrium phase diagram, carbon diffuses interstitially on cooling, into ferrite, thereby ensuring complete distribution of all the alloying elements including carbon.

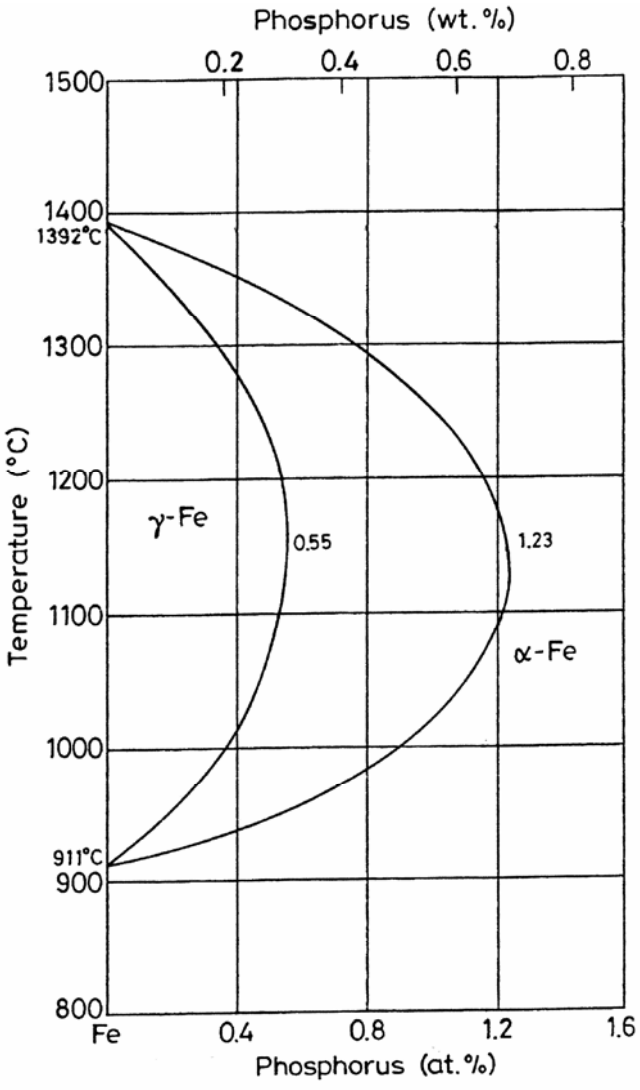

Figure 4. High temperature gamma loop region of the Fe–P phase diagram (Kubaschewski 1982).

Mild steel encapsulation was then removed by machining. The slabs, after removal of mild steel skin, were hot rolled using flat roll at 900°C to make thin sheets. Rolling was carried out very slowly at 900°C with 0·1 mm thickness reduction per pass. The rolling was done using small laboratory scale rolling mill with 10 cm roll diameter. The sheets were then vacuum annealed at 950°C for 40 min to relieve the residual stresses. All the samples prepared this way were characterized in terms of density, microstructure, hardness, and tensile properties as detailed elsewhere (Trivedi *et al* 2009).

The samples (15 mm length, 15 mm width, and 2 mm thickness) for electrochemical testing were cut along the rolling direction. The surfaces were finished using SiC abrasive paper (up to 800 grit) and samples were degreased with acetone. Several samples were prepared from the starting materials for conducting reproducible experiments. One side of the samples was soldered with a copper wire. Then the soldered sample was covered with enamel exposing an area of 1 cm^2. The samples were mounted in a K0047 Corrosion Cell (used in ASTM standard G-5, supplied by Ametek, USA) for conducting Tafel polarization studies at a scan rate of 0·166 mV/s. The Tafel extrapolation method (conducted as per ASTM Standard G3-89, 2006) was utilized for determining i_{corr} of the phosphoric irons and Armco electrolytic iron in 0·25 M H_2SO_4 of pH 0·6 and 3·5% NaCl having pH 6·8.

Since the cathodic reaction was primarily diffusion controlled in the case of 3·5% NaCl solution having pH 6·8, the activation-controlled anodic Tafel region was extrapolated to intersect the horizontal drawn at zero current potential to obtain the corrosion rate (ASTM Standard G102-89, 2006).

Linear polarization technique was used to evaluate the corrosion rates of the phosphoric irons and Armco electrolytic iron in the following solution: 0·5 M Na_2CO_3 + 1·0 M $NaHCO_3$ solution of pH 9·4. A scan rate of 0·166 mV/s was used. Corrosion rate in penetration units (like mils/year, mpy), was calculated from i_{corr} using the following equation (Ijsseling 1986):

$$\text{mpy} = i_{corr} \times \Lambda \times 1/\rho \times \varepsilon,$$

where $\Lambda = 128660$ (equivalents.s.mil)/(Coulombs.cm.years), i_{corr} the corrosion current density in amps/sq. cm (amp = 1 coulomb/s), ρ the density (7·86 g/cubic cm, for iron) and ε the equivalent weight (27·56 g/equivalent, for iron).

The solutions were prepared using chemicals of analytical grade reagent and single distilled water. A digital pH meter (Phillips, model 9045) was used for recording pH of the solutions at room temperature. The pH meter was

Table 2. Corrosion data for phosphoric irons in 0·25 M H_2SO_4 solution (0·6 pH).

Sample	Beta anodic (V/decade)	Beta cathodic (V/decade)	E_{corr} vs SCE (mV)	I_{corr} (μA)	Corrosion rate (mpy)
1	509·0E33	–181·9E-3	–553·0	174·7	78·8
2	324·2E-3	–140·6E-3	–480·2	243·5	109·89
3	16·53E3	–121·3E-3	–481·3	93·07	41·98

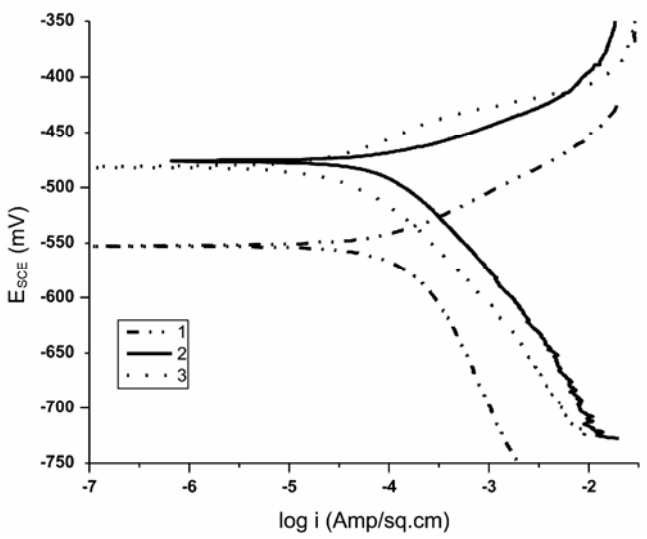

Figure 5. Tafel curves for the samples in 0·25 M H_2SO_4 solution (0·6 pH).

calibrated using three different standard pH solutions before recording pH.

An EG and G PARSTAT 273A Potentiostat (Ametek, USA) and a saturated calomel reference electrode (SCE) were used in all electrochemical experiments. The open circuit potential (OCP) was stabilized for 1 h before the start of each experiment. All the experiments were repeated three times.

3. Results and discussion

The corrosion rates determined by the Tafel extrapolation method in aerated solutions of 0·25 M H_2SO_4 of pH 0·6 and 3·5% NaCl of pH 6·8 and those determined by the linear polarization method in an aerated solution of 0·5 M Na_2CO_3 + 1·0 M $NaHCO_3$ of pH 9·4 are discussed separately below. The cathodic reaction for the samples obtained in all the three solutions discussed above consists of a composite reaction of (Flitt and Schweinsberg 2005) hydrogen evolution

$$2H^+ + 2e^- \rightarrow H_2$$

$$2H_2O + 2e^- \rightarrow H_2 + 2OH.$$

And oxygen reduction

$$½\ O_2 + H_2O + 2e^- \rightarrow 2OH.$$

This is also evident from Pourbaix diagram of the Fe–H_2O system.

3.1 *Tafel extrapolation method*

3.1a *0·25 M H_2SO_4 solution (pH 0·6)*: As pH decreases, hydrogen evolution rate will dominate over oxygen reduction rate at E_{corr}. Thus, at pH 0·6, the contribution of hydrogen evolution at E_{corr} is significant. The exchange current density, i_0, for hydrogen evolution, H^+/H_2 and i_{corr}, increase on increasing the concentration of H^+ ion or decreasing the pH (Davydov *et al* 2005). Hence corrosion rate increases.

The beta anodic and cathodic slopes, E_{corr}, i_{corr} and corrosion rate (mpy) obtained from the Tafel curves of the samples are tabulated in table 2 and displayed in figure 5. The E_{corr} lies between –480 mV_{sce} and –482 mV_{sce}. The corrosion rate for sample 3 is 40 mpy. This is similar to that obtained for copper-chromium based corrosion resistant TATA steel (46 mpy). The corrosion rate for sample 2 is 110 mpy and is much less than that obtained for plain carbon steel (250 mpy) (Sahoo and Balasubramaniam 2008).

3.1b *3·5% NaCl solution (pH 6·8)*: The Tafel plots obtained in aerated 3·5% NaCl solution are shown in figure 6. Tafel polarization curves showed diffusion controlled cathodic reaction in all cases. In this case, the diffusion-controlled oxygen reduction reaction is the dominant reaction at E_{corr} (Flitt and Schweinsberg 2005). The activation controlled anodic Tafel slopes, i_{corr} and corrosion rate (mpy) obtained from the Tafel polarization curves of samples (figure 6) are tabulated in table 3. Since the cathodic reaction is diffusion controlled, hence the cathodic Tafel slopes are not provided in table 3 (ASTM Standard G102-89, 2006).

The corrosion rate was obtained from the Tafel extrapolation method matched with literature data, as discussed below. The corrosion rate of samples obtained by the Tafel extrapolation method after 1 h immersion in 3·5% NaCl was in the range of 6–10 mpy (Sahoo and Balasubramaniam 2008).

In the present study, the corrosion rate of samples obtained by the Tafel extrapolation method after 1 h immersion in 3·5% NaCl was in the range of 1·5–2·5 mpy. The E_{corr} of the samples lies between –450 mV_{SCE} and –542 mV_{SCE}. Hence these samples are most suitable for marine environments.

3.2 *Linear polarization method*

3.2a *0·5 M Na_2CO_3 + 1·0 M $NaHCO_3$ solution (pH 9·4):* The R_p, E_{corr}, i_{corr} and corrosion rate (mpy) obtained from the linear polarization curves of samples are tabulated in table 4 and displayed in figure 7. The E_{corr} lies between –220 mV_{sce} and –230 mV_{sce}. The corrosion rate is low and lies between 0·2 and 0·35 mpy (mils per year). These materials are suitable in buried (in soil) conditions. This solution was chosen to evaluate the corrosion resistance of the samples against soil (buried condition). Alkaline solutions are known to cause intergranular SCC due to segregation of phosphorous in low alloy steels (Sikora *et al* 1993). The corrosion rate of phosphoric irons is low and lies between 2 and 8 mpy (mils per year) (Mehta *et al* 2009).

Table 3. Corrosion data (Tafel) for phosphoric irons in 3·5% NaCl solution (6·8 pH)

Sample	Beta anodic (V/decade)	E_{corr} vs SCE (mV)	I_{corr} (μA)	Corrosion rate (mpy)
1	67·08E-3	–424·6	2·897	1·3
2	43·35E-3	–542·7	5·258	2·4
3	22·27E-3	–451·6	3·204	1·4

Table 4. Corrosion data (linear polarization) for phosphoric irons in 0·5 M Na_2CO_3 + 1·0 M $NaHCO_3$ solution (9·4 pH).

Sample	R_p (Ohms)	E_{corr} vs SCE (mV)	I_{corr} (μA)	Corrosion rate (mpy)
1	89600	–252	0·2424	0·11
2	283400	–221·1	0·7662	0·34
3	475800	–228·2	0·4563	0·2

3.3 *Segregation of alloying elements*

Powder metallurgical phosphoric irons developed in the present investigation are free of any segregation of the alloying elements along the grain boundaries. They get distributed uniformly in the entire structure. This has been confirmed by: (i) optical microscope (figure 8), (ii) surface morphology (SEM) and EDAX pattern from different spots (figures 9 and 10), and (iii) composition image [secondary image] and X-ray mapping (figure 11).

The optical micrographs show that the pores are elongated in the direction of rolling. The pores are found predominantly in the interior of the grains. The pores appear larger than their actual size due to the effect of etching. All the grains belong to a single phase that is ferrite. No other phase can be detected.

The SEM photos reveal that the grains are of a single phase. There is no second phase. The pores are away from the grain boundaries which is good for the mechanical properties. The microstructures are very similar. This is because the two compositions differ from each other marginally i.e. by 0·15% C.

The analysis of surface morphology and EDAX pattern from different spots reveals that the elements are distributed more or less evenly in the grain interiors and at the grain boundaries. This data should not be interpreted in the absolute sense. They can be utilized for comparison purposes, at best.

In this respect, C, Cu and Ni are austenite stabilizers and Mo, Si and P are ferrite stabilizers. When the mixture

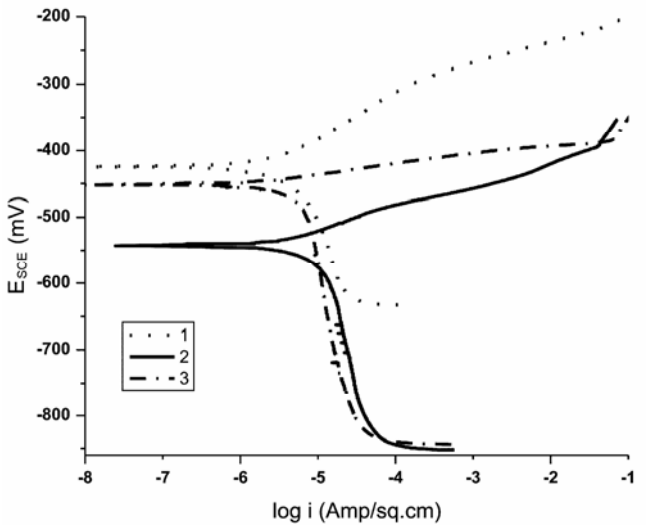

Figure 6. Tafel curves for the samples in 3·5% NaCl solution (6·8 pH).

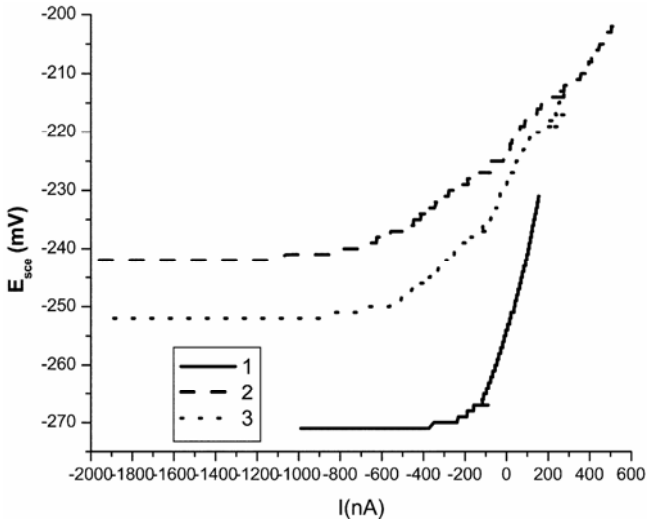

Figure 7. Linear polarization curves for the samples in 0·5 M Na_2CO_3 + 1·0 M $NaHCO_3$ solution (9·4 pH).

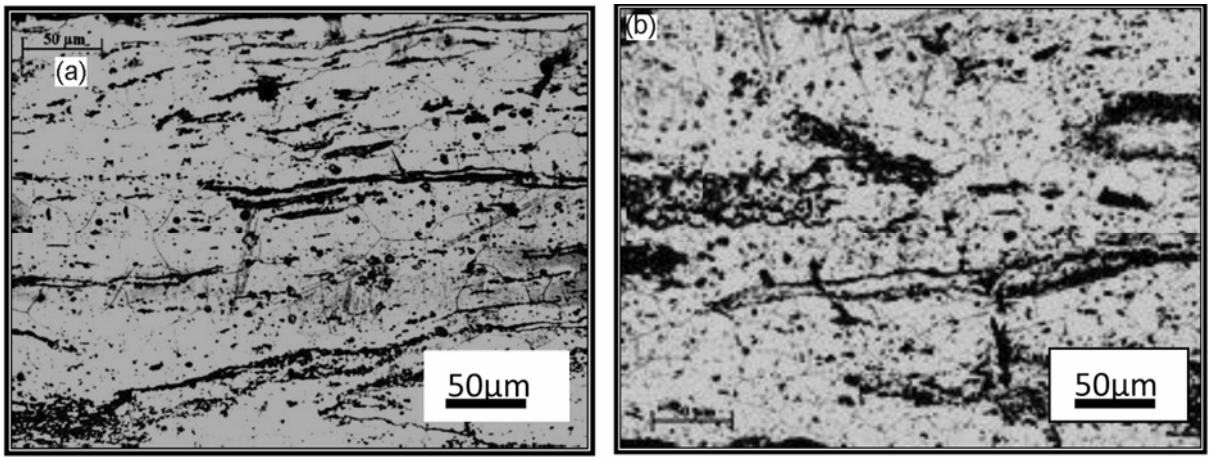

Figure 8. Microstructures of rolled and annealed alloys etched with 2% Nital. Pores are elongated in the rolling direction. (**a**) Sample 2 and (**b**) sample 3.

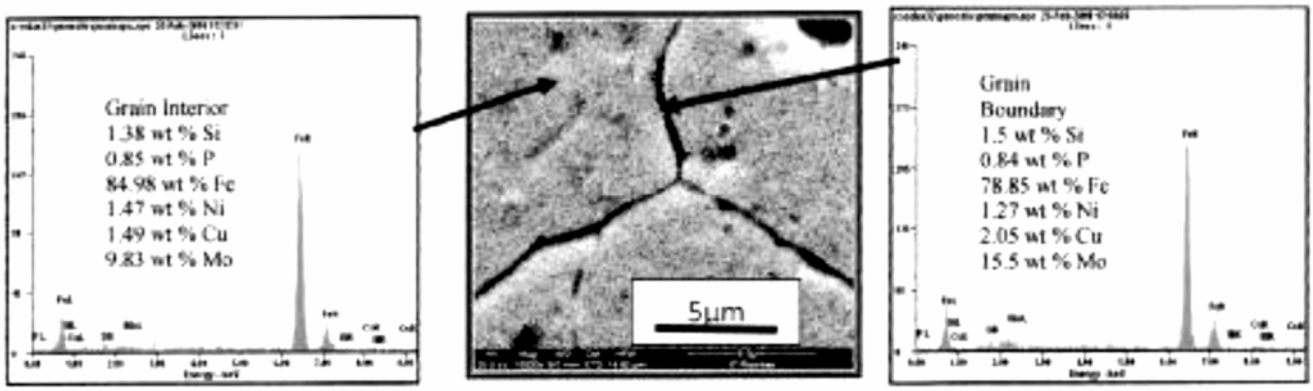

Figure 9. Surface morphology and EDAX pattern from different spots on sample 2.

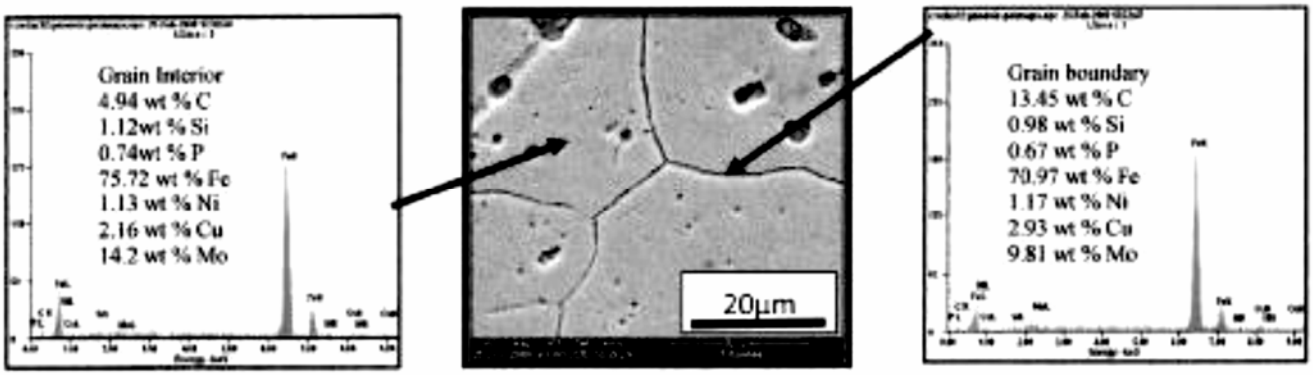

Figure 10. Surface morphology and EDAX pattern from different spots on sample 3.

of powders is subjected to consolidation, employing high temperature and pressure, it will undergo phase transformation. Fe powder particles would first convert to gamma (*fcc*) iron and as ferrite stabilizers diffuse inside, they would gradually convert into alpha (*bcc*) iron. In this way, transfer of all the ferrite stabilizers would proceed from Fe particle surfaces towards the interior of the particles. However, C, Cu and Ni have low solubility in alpha would not be able to diffuse in preference to alpha stabilizers. Thus Fe powder particle surfaces would be con-

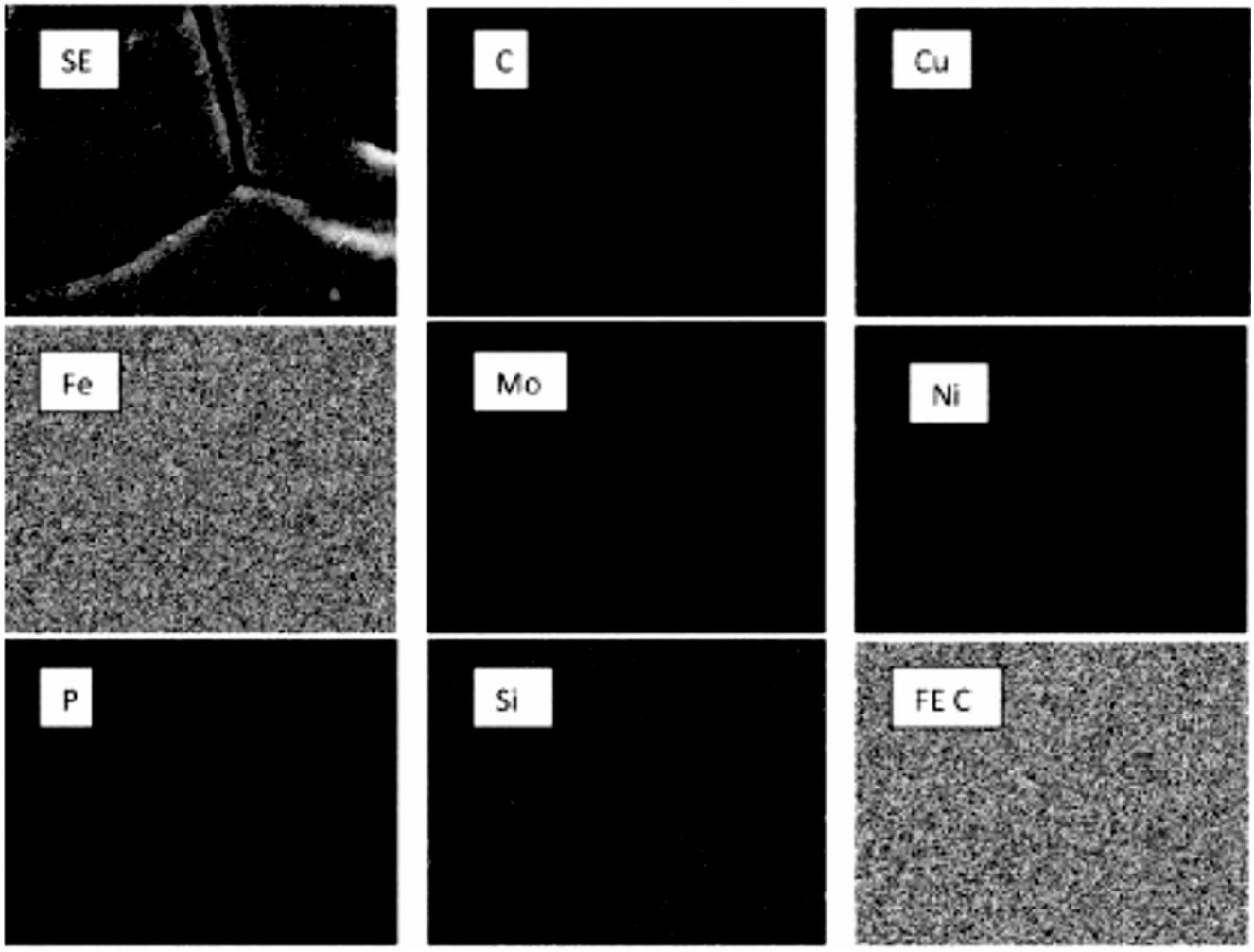

Figure 11. Composition image [secondary image] and X-ray mapping of sample 3.

centrated with C, Cu and Ni and would remain austenitic at the temperature of forging. These particle surfaces ultimately get converted into grain boundary where we find higher concentrations of C, Cu and Ni in comparison to the grain interior. Whereas, the grain boundaries are depleted in Mo, Si and P contents as a major amount has diffused into the grain interior. X-ray mapping of all the elements confirms that these elements get distributed uniformly in the entire structure showing no signs of segregation, of any alloying element.

Further, residual porosity in these samples (of the order of 2 vol %) has no adverse effect under moderate corrosion conditions as described above.

4. Conclusions

(I) Ordinarily, powder metallurgical alloys are poor in corrosion resistance due to the inherent porosity associated with them. However, phosphoric irons alloyed with ferrite formers such as silicon, offer improved corrosion resistance in general, as compared with known wrought based iron systems.

(II) Carbon addition in iron–phosphorous powder metallurgical alloys lower corrosion rates in the range of pH 0·6–9·4.

(III) The compositions designed in this investigation are preferable under alkaline conditions.

(IV) These alloys can also be used under marine/de-icing salt conditions.

References

Balasubramaniam R 2000 *Corros. Sci.* **42** 2103

Balasubramaniam R 2002 *Delhi iron pillar: New insight* (New Delhi: Indian Institute of Advanced Studies and Aryan Books International) pp 138–139

Balasubramaniam R and Ramesh Kumar A V 2000 *Corros. Sci.* **42** 2085

Davydov A, Rybalka V, Beketaeva L, Engelhardt G, Jayaweera P and Macdonald D 2005 *Corros. Sci.* **47** 195

Erhart H and Grabke H 1981 *J. Met. Sci.* **15** 401
Flitt H J and Schweinsberg D 2005 *Corros. Sci*. **47** 3034
Fontana M G 2006 *Corrosion engineering* (New Delhi: Tata-McGraw-Hill) 3rd ed, pp 23–27 and pp 499–503
Ijsseling F P 1986 *Br. Corros. J. London* **21** 95
Kubaschewski O 1982 *Iron—Binary phase diagrams* (Berlin: Springer Verlag) pp 84–86
Lorbeer P and Lorenz W J 1980 *Electrochim. Acta* **25** 375
Mehta Y, Trivedi S, Chandra K and Mishra P S 2009 *J. Miner. & Mater. Charact. & Eng.* (accepted)
Nishimura T 2008 *Sci. Technol. Adv. Mater.* **9** 1
Oakwood T G 1987 *ASM Handbook Corrosion* (Metals Park, OH: ASM International) **Vol. 13** p 532
Sahoo G and Balasubramaniam R 2008 *J. ASTM Int.* **5** 1
Sands R L and Shakespeare C R 1966 *Powder metallurgy—Practice and applications* (UK: George Newnes Ltd) pp 112–114
Sikora E, Sadkowski A and Flis J 1993 *Electrochim. Acta* **38** 2443
Trivedi S, Mehta Y, Chandra K and Mishra P S 2010 *J. Mater. Process. Technol.* **210** 85